NASA CONTRACTOR REPORT

NASA CR-779

AN INTEGRAL EQUATION METHOD IN PLANE ELASTICITY

by Kwan Rim and Allen S. Henry

Prepared by
THE UNIVERSITY OF IOWA
Iowa City, Iowa
for

NATIONAL AERONAUTICS AND SPACE ADMINISTRATION • WASHINGTON, D. C. • MAY 1967

NASA CR-779

AN INTEGRAL EQUATION METHOD IN PLANE ELASTICITY

By Kwan Rim and Allen S. Henry

Prepared under Grant No. NsG-576 by
THE UNIVERSITY OF IOWA
Iowa City, Iowa

for

NATIONAL AERONAUTICS AND SPACE ADMINISTRATION

For sale by the Clearinghouse for Federal Scientific and Technical Information
Springfield, Virginia 22151 – CFSTI price $3.00

TABLE OF CONTENTS

AN INTEGRAL EQUATION METHOD IN PLANE ELASTICITY

By Kwan Rim and Allen S. Henry

Department of Mechanics and Hydraulics
The University of Iowa
Iowa City, Iowa

SUMMARY

A direct numerical method is developed for solving the first fundamental boundary-value problem of plane elastostatics. The method is based on the formulation of the biharmonic stress function in terms of two harmonic functions and the subsequent representation of the harmonic functions as potential functions, each containing an unknown source density function. The boundary conditions yield two coupled integral equations of the Fredholm type, the solution of which determines the source density functions.

Numerical solutions for the unknown source densities are determined by approximating the Fredholm equations by sets of simultaneous algebraic equations which may be set up and solved by a high-speed digital computer. Once the source density functions are known, stresses may be calculated anywhere in the elastic domain. Numerical illustrations are presented for a circular region loaded with diametrally opposite concentrated forces and for an infinite domain with an elliptic internal boundary subjected to a constant pressure.

INTRODUCTION

The purpose of this report is to present a direct numerical method for solving the first fundamental boundary-value problem of plane elastostatics. The essence of the method is to develop solutions to two coupled integral equations of the Fredholm type. These equations arise from the requirement that a biharmonic stress function, represented in terms of single-layer potentials, must satisfy certain specified conditions on the boundary. The basis of the numerical technique lies in the replacement of the integral equations by sets of algebraic equations.

In both the formulation and practical implementation of the method, there are no restrictions on the geometry of the region except that the boundary contours must be piece-wise smooth and that it is necessary to distinguish between problems involving

1) Interior domains,
2) Exterior domains,
3) Multiply-connected domains.

The factors permitting such an unusual degree of generality will be emphasized as they appear in the following sections of this report.

A discussion of the fundamental theory relating to this integral equation method may be found in a paper by Jaswon (ref. 1) which presents a study of Fredholm equations related to harmonic and biharmonic boundary-value problems. A sequel to Jaswon's paper (ref. 2) describes a numerical technique developed to obtain approximate solutions to Fredholm equations. Numerical results are presented for certain harmonic problems. A third paper (ref. 3) illustrates an application of the method by computing solutions to the classical torsion problem and extensive numerical results are given. Finally a dissertation by Symm (ref. 4) provides a thorough theoretical discussion and numerical results for several harmonic and biharmonic problems.

The research reported herein is an extension of the work reported in the above papers and is specifically concerned with exploiting fully the numerical technique in determining stress fields in interior and exterior domains. The numerical examples chosen serve to illustrate the effect of boundary loading and geometry on the accuracy of numerical results. The interior problem treated is a circular disk subjected to diametrally opposite concentrated forces. The exterior problem is an infinite medium with an elliptic hole subjected to uniform pressure. In this case, results are presented for various eccentricities. Particular attention is paid to the accuracy of the computed boundary stresses, since it may serve as a measure of convergence.

In the following section, the theoretical basis of the method is outlined in discussing the interior problem. No attempt is made to discuss the questions of existence and uniqueness of solutions as such discussions may be found in the literature (refs. 1 and 4). Then the exterior problem and the computational technique are treated. Finally, numerical results are presented and several conclusions are induced. In this report, only the first fundamental boundary-value problems in plane elastostatics are discussed, and no problems of multiply-connected domains are treated.

SYMBOLS

D	a planar domain bounded by a closed curve L.
P	a vector point in D with coordinates (x,y).
p, q	vector points on L with coordinates (x,y) and (x_q, y_q), respectively. (note that $p \neq P$)
$\bar{n}$, $\bar{s}$	unit vectors normal and tangent to L.
χ	a stress function biharmonic in D.
ϕ, ψ	harmonic functions in D.
σ, μ	source densities defined on L.
$\log \lvert P-q \rvert$	the natural logarithm of the scalar distance between $P(x,y)$ and $q(x_q, y_q)$.
σ_x, σ_y, τ_{xy}	stress components.
θ	total stress, $\theta = \sigma_x + \sigma_y$.
F_x, F_y	x- and y- components of the stress vector on L respectively.
∇^2	Laplace's operator $\nabla^2 = \frac{\partial^2}{\partial x^2} + \frac{\partial^2}{\partial y^2}$.

BASIC THEORY: THE INTERIOR PROBLEM

The problem of determining the stress field in a planar region, subjected to specified boundary loadings, may be posed mathematically as one of finding a stress function χ which is related to the stress components by the equations

$$\sigma_x = \frac{\partial^2 \chi}{\partial y^2}, \qquad \sigma_y = \frac{\partial^2 \chi}{\partial x^2}, \qquad \tau_{xy} = -\frac{\partial^2 \chi}{\partial x \partial y} \tag{1}$$

The stress function will satisfy the compatibility and the equilibrium equation provided that it is a solution to the biharmonic equation within the region of interest;

$$\nabla^2 \nabla^2 \chi(P) = 0, \qquad P(x,y) \text{ in } D. \tag{2}$$

The stress components defined by (1) must be consistent with the state of stress specified on the boundary L of the domain D. If F_x and F_y are the stress components in the x and y directions specified on L, then the boundary conditions may be written, using equations (1), as

$$\left.\begin{aligned} -F_x &= \frac{\partial x}{\partial n}\frac{\partial^2 \chi}{\partial y^2} - \frac{\partial y}{\partial n}\frac{\partial^2 \chi}{\partial x \partial y} \\ -F_y &= \frac{\partial y}{\partial n}\frac{\partial^2 \chi}{\partial x^2} - \frac{\partial x}{\partial n}\frac{\partial^2 \chi}{\partial x \partial y} \end{aligned}\right\} \text{ on } L \tag{3}$$

where $\bar{n}$ is the normal to L directed inward toward D. The notation employed is depicted in figure 1.

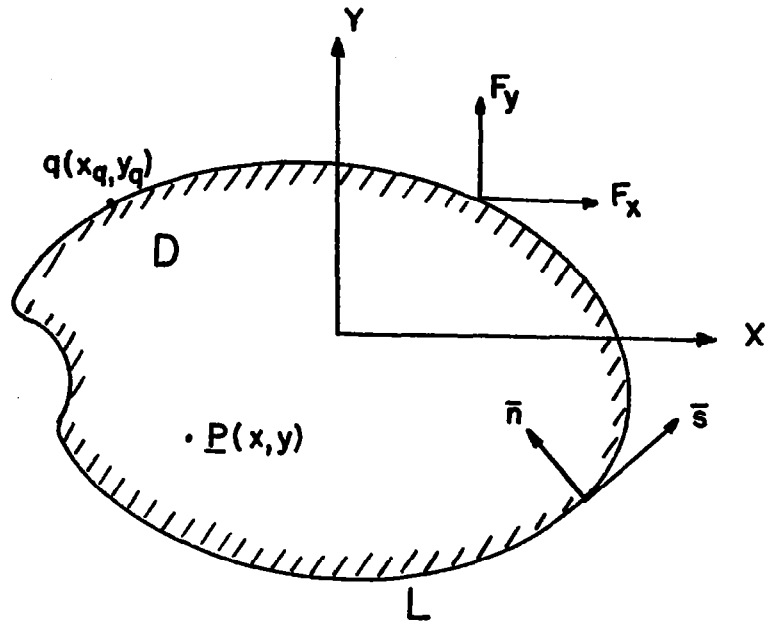

Figure 1.- Sign convention for an interior domain.

The basic mathematical problem posed is that of finding a solution χ to equation (2) which satisfies the boundary conditions (3). The approach taken herein is to first present a general solution for $\chi(P)$ which satisfies (2), and then develop a numerical scheme for fitting the general solution to the boundary conditions (3).

A general representation for a biharmonic function is

$$\chi(P) = r^2(P)\,\phi(P) + \psi(P) \tag{4}$$

where $r(P) = (x^2 + y^2)^{\frac{1}{2}}$ and ϕ and ψ are harmonic functions;

$$\nabla^2\phi(P) = 0\,, \qquad \nabla^2\psi(P) = 0\,; \quad P \text{ in } D\,.$$

The single-layer potentials

$$\phi(P) = \int_L \sigma(q)\,\log|P - q|\,dq \tag{5}$$

and

$$\psi(P) = \int_L \mu(q)\,\log|P - q|\,dq \tag{6}$$

are both harmonic within D as σ and μ are defined only on L and $\log|P - q|$ is harmonic. Integration is over the entire boundary and dq is a scalar element of arc on L. Substitution of (5) and (6) into (4) yields

$$\chi(P) = r^2(P)\int_L \sigma(q)\log|P - q|dq + \int_L \mu(q)\log|P - q|dq \qquad (7)$$

which is a biharmonic function involving two unknown functions σ and μ, commonly termed "source density" functions. The properties of this representation are available in the literature (refs. 1, 2, 3 and 4) and the representation for χ given by (7) is complete only for simply-connected interior domains.

An examination of (7) indicates that the use of the boundary conditions as presented by (3) is awkward, for these equations require that representations be developed for the second derivatives of χ. Hence the boundary conditions (3) are used to derive conditions for χ and $\frac{\partial\chi}{\partial n}$ on the boundary L. If the tangent to L, $\bar{s}$, is directed so as to keep D on the left, then (3) may be written, using the Cauchy-Riemann conditions, as

$$F_x = \frac{d}{ds}\left(\frac{\partial\chi}{\partial y}\right), \qquad F_y = -\frac{d}{ds}\left(\frac{\partial\chi}{\partial x}\right).$$

Then since

$$\frac{\partial\chi}{\partial s} = \frac{\partial\chi}{\partial x}\frac{\partial x}{\partial s} + \frac{\partial\chi}{\partial y}\frac{\partial y}{\partial s},$$

direct substitution and integration yield

$$\chi(s) = -\int_{s_0}^{s}\frac{\partial x}{\partial s}\left[\int_{s_0}^{s} F_y ds\right]ds + \int_{s_0}^{s}\frac{\partial y}{\partial s}\left[\int_{s_0}^{s} F_x ds\right]ds + \alpha x + \beta y + \gamma \qquad (8)$$

also it follows that

$$\frac{\partial\chi(s)}{\partial n} = -\frac{\partial x}{\partial n}\int_{s_0}^{s} F_y ds + \frac{\partial y}{\partial n}\int_{s_0}^{s} F_x ds + \alpha\frac{\partial x}{\partial n} + \beta\frac{\partial y}{\partial n}, \qquad (9)$$

where s is on the boundary L; s_0 designates an arbitrary point on L and α, β and γ are constants of integration which may be set to zero as they make no contribution to the stress field.

Note that equations (8) and (9) permit χ and $\frac{\partial \chi}{\partial n}$ to be computed directly once the boundary tractions and the boundary geometry are specified.

The boundary value problem originally defined by (2) and (3) is now presented in canonical form by (2), (8) and (9). Since the representation of χ provided by (7) automatically satisfies (2), the boundary value problem is solved formally by requiring (7) to satisfy (8) and (9). These two boundary equations lead to two coupled integral equations for the determination of $\sigma(q)$ and $\mu(q)$. It is generally impossible to solve the coupled integral equations exactly, hence a numerical method is developed for obtaining approximate solutions.

The fundamental approximation is to assume that the source densities σ and μ are piece-wise constant functions on the boundary L. Hence the boundary is divided into m subdivisions or intervals numbered consecutively in the direction of increasing s, and within each interval $\sigma(q)$ and $\mu(q)$ are assigned the unknown constant values σ_i and μ_i $(i = 1, 2, \ldots m)$. The i-th interval is assigned length h_i and the center and end points are denoted q_i, $q_{i-1/2}$ and $q_{i+1/2}$. This situation is depicted in figure 2. In accordance with these assumptions, equation (7) becomes

$$\chi(P) = r^2(P) \sum_{i=1}^{m} \sigma_i \int_i \log|P - q| dq + \sum_{i=1}^{m} \mu_i \int_i \log|P - q| dq \qquad (10)$$

where integration is over the i-th interval.

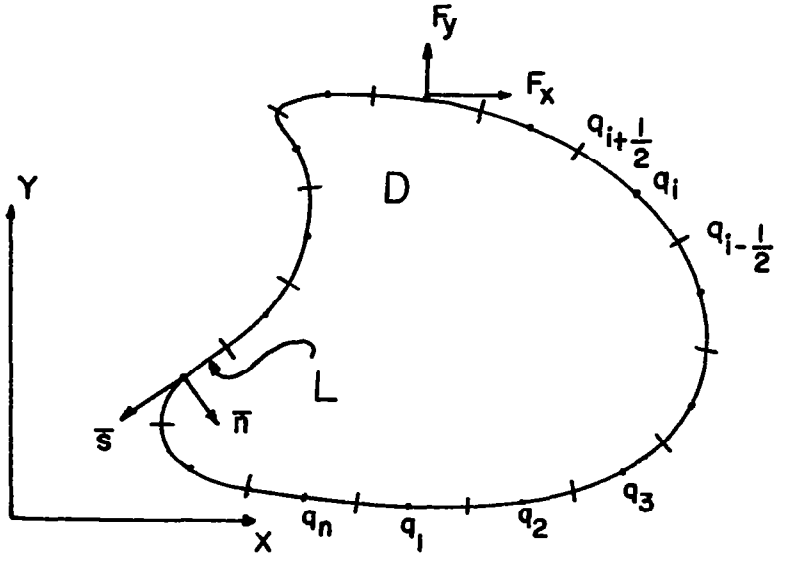

Figure 2.- Boundary subdivisions.

Finally, the stress function $\chi(P)$ given by (10) is required to satisfy the boundary conditions (8 and 9) at the center point of each interval. If the center point of the j-th interval is also denoted by p_j, then

$$\lim_{P\to p} \int_L \sigma(q)\log|P - q|dq = \int_L \sigma(q)\log|p - q|dq$$

and $$\lim_{P\to p} \frac{\partial}{\partial n} \int_L \sigma(q)\log|P - q|dq = \pi\sigma(p) \frac{\partial x}{\partial n} + \int_L \sigma(q)\log'|p - q|dq ,$$

where $$\log'|p - q| = \frac{\partial}{\partial n(p)} \log|p - q| .$$

Hence the simultaneous equations for σ_j and μ_j become

$$\chi(p_j) = r^2(p_j) \sum_{i=1}^{m} \sigma_i \int_i \log|p_j - q|dq + \sum_{i=1}^{m} \mu_i \int_i \log|p_j - q|dq \qquad (11)$$

$$\frac{\partial\chi(p_j)}{\partial n} = \pi[r^2(p_j)\sigma(p_j) + \mu(p_j)] + 2 \frac{\partial r(p_j)}{\partial n} \sum_{i=1}^{m} \sigma_i \int_i \log|p_j - q|dq$$

$$+ r^2(p_j) \sum_{i=1}^{m} \sigma_i \int_i \log'|p_j - q|dq + \sum_{i=1}^{m} \mu_i \int_i \log'|p_j - q|dq , \qquad (12)$$

where $j = 1, 2, 3, \ldots m$. For simplification, one may introduce the following notations:

$$A_{ji} = \int_i \log|p_j - q|dq , \quad B_{ji} = \int_i \log'|p_j - q|dq .$$

Since $\chi(p_j)$ and $\frac{\partial\chi(p_j)}{\partial n}$ are known from (8) and (9), relations (11) and (12) represent 2m equations for 2m unknowns σ_i and μ_i ($i = 1, 2, \ldots m$). Once the σ_i and μ_i are known, the stresses may be determined by differentiating (10) and performing the required calculations.

The preceding analysis is adequate for the treatment of interior problems; that is, the representation provided by (7) is complete and the solutions of (11) and (12) lead to a unique stress function $\chi(P)$. As will be seen,

however, slight changes are required in the treatment of the exterior problem.

THE EXTERIOR PROBLEM

In order to solve the problem of determining stresses in an infinite elastic domain with an interior boundary, a slight change is required in the representation of the stress function. Consideration of (7) shows that as $|P|$ goes to infinity, one has

$$\chi(P) \to r^2(P)\log|P| \int_L \sigma(q)dq + \log|P| \int_L \mu(q)dq \ . \tag{13}$$

An analysis of the relation between $\chi(P)$ and the displacements associated with the stress field shows that in order for these displacements to be single-valued the stress function cannot contain the term $r^2(P)\log|P|$ (refs. 1 and 4). Hence, from (13), it follows that

$$\int_L \sigma(q)dq = 0 \ .$$

A result of imposing this constraint on the representation of χ given by (7) is that $\chi(P)$ is of order $|P|$ as $|P| \to \infty$. Hence all stress components will approach zero as $|P|$ goes to infinity. Therefore, if a problem requires that non-zero stresses exist at infinity, additional terms which satisfy these conditions must be added to χ as given by (7). Finally it may be shown from (13) that (7) does not permit χ to contain a constant term as is required in the most general representation of a biharmonic function. Therefore, the addition of an arbitrary constant A to the representation provided by (7) is required.

With these modifications implemented, a necessary and sufficient representation of the stress function for an exterior problem is

$$\chi(P) = r^2(P) \int_L \sigma(q)\log|P - q|dq + \int_L \mu(q)\log|P - q|dq + A \tag{14}$$

with the additional condition that

$$\int_L \sigma(q)dq = 0 \ .$$

Assuming $\sigma(q)$ and $\mu(q)$ to be piecewise constant on L and requiring that χ and its normal derivative satisfy conditions at the m interval center points leads directly to $2m + 1$ equations in the $2m + 1$ unknowns A, σ_i and μ_i; $i = 1, 2, \ldots m$. These equations are identical to the set of equations given by (11) and (12) except for the inclusion of the constant A and the condition that

$$0 = \sum_{i=1}^{m} \sigma_i h_i .$$

Except for the modifications indicated above, the interior and exterior problems can be treated in identical fashion. In the next section, a discussion is given concerning the computational technique used to determine the source densities and to compute the stress components.

COMPUTATIONAL TECHNIQUE

For the purpose of illustration, let us consider the equations which must be solved to determine the stress function applicable to an exterior problem. These equations are:

$$\sum_{i=1}^{m} \sigma_i r^2(p_j) A_{ji} + \sum_{i=1}^{m} \mu_i A_{ji} + A = \chi(p_j) \tag{15}$$

$$\sum_{i=1}^{m} \sigma_i [\pi r^2(p_j)\delta_{ij} + r^2(p_j) B_{ji} + (r^2(p_j))' A_{ji}] + \sum_{i=1}^{m} \mu_i (\pi\delta_{ij} + B_{ji}) = \chi'(p_j) \tag{16}$$

$$\sum_{i=1}^{m} \sigma_i h_i = 0 \qquad (j = 1, 2, \ldots m) \tag{17}$$

where

$$A_{ji} = \int_i \log|p_j - q| dq$$

$$B_{ji} = \int_i \log'|p_j - q| dq$$

$$\delta_{ij} = \begin{cases} 1, & i = j \\ 0, & i \neq j \end{cases}.$$

Recall that $\chi(p_j)$ and $\chi'(p_j)$ can be calculated from specified data; that is, the geometry and the loading conditions of the boundary. Then the

first task in seeking solutions to (15), (16) and (17) is to evaluate A_{ji} and B_{ji}. In general, exact expressions for these quantities cannot be obtained; therefore, approximate integration formulas are used to evaluate these coefficients. The use of approximate formulas has the advantage that these formulas may be programmed on a digital computer and used for all problems thus preserving the generality of the method.

The use of approximate integration formulas for the cases where the integrands are non-singular $(i \neq j)$ is justifiable as these formulas may be more accurate than the original assumption that $\sigma(q)$ and $\mu(q)$ are piecewise constant on L. When the integration is made over the j-th interval $(i = j)$, then $\log|p_j - q|$ and $\log'|p_j - q|$ are singular at $q = p_j$. In these instances, analytic estimates of the integral are obtained by approximating the j-th interval by either straight line segments or a circular arc. In presenting these formulas, the notations in figures 1 and 2 are used except that for the exterior problem the directions of $\bar{n}$ and $\bar{s}$ are reversed.

For $i \neq j$, Simpson's rule gives

$$A_{ji} \doteq \frac{h_i}{6}\left[\log|p_j - q_{i-1/2}| + 4\log|p_j - q_i| + \log|p_j - q_{i+1/2}|\right] \tag{18}$$

while a simpler formula yields

$$B_{ji} \doteq h_i \log'|p_j - q_i| \,, \tag{19}$$

where

$$\log'|p_j - q_i| = \frac{(x_j - x_{q_i})\frac{\partial x}{\partial n} + (y_j - y_{q_i})\frac{\partial y}{\partial n}}{|p_j - q_i|^2} \,.$$

If $i = j$, the j-th interval is approximated by two straight line segments joining $q_{j-1/2}$ to q_j and q_j to $q_{j+1/2}$. Then analytic integration yields

$$A_{jj} \doteq |q_j - q_{j-1/2}|\left[\log|q_j - q_{j-1/2}| - 1\right] + |q_j - q_{j+1/2}|\left[\log|q_j - q_{j+1/2}| - 1\right] \tag{20}$$

To obtain an analytic estimate for B_{jj}, the j-th interval is approximated by a circular arc. For this case, since

$$\log'|p_j - q| = \log|p_j - q|' ,$$

using the Cauchy-Riemann conditions it can be shown that

$$B_{jj} = -\int_j \frac{d\Omega(|p_j - q|)}{ds}\, dq \tag{21}$$

where $\Omega(|p_j - q|)$ is the angle between the line segment $|p_j - q|$ and any prescribed datum. Note that this integral is improper

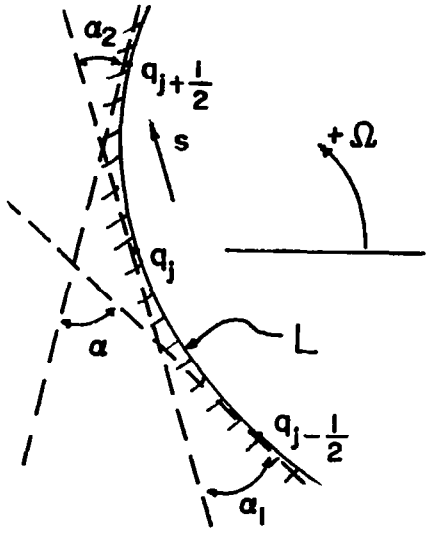

Note: Dashed lines are tangents to L.

$$\int_j \frac{d\Omega}{ds}(|p_j - q|)\, dq = -(\alpha_1 + \alpha_2)$$

Figure 3.- Determination of B_{jj}.

as Ω is discontinuous at $q = p_j$, hence the integration does not extend over the discontinuity. Figure 3 shows the geometry associated with this integration.

From figure 3 it is seen that

$$B_{jj} = \begin{cases} \alpha & \text{for exterior problems} \\ -\alpha & \text{for interior problems,} \end{cases} \tag{21a}$$

where α can be computed from the law of cosines. The data required for approximations (18) through (21) are the coordinates of the interval end and center points, $\frac{dx}{dn}$ and $\frac{dy}{dn}$ at the interval center points, and the interval lengths h_i .

The calculation of source densities is now reduced to a straightforward procedure which begins with the computation of constants A_{ji} and B_{ji} with equations (18) through (21a) . For an interior problem, these constants are substituted into equations (11) and (12) which are solved for the 2m unknowns σ_i and μ_i , $i = 1, 2, \ldots m$. An exterior problem is handled in a like manner with equations (15), (16) and (17) .

To calculate stresses in D one differentiates (14) or (7) in accordance with (1) and performs the indicated computations. The integrals appearing in the formulas for stress components are approximated by Simpson's rule, as all integrals are continuous if P lies within D (not on L). The accuracy of integration formulas is illustrated in Appendix A.

The calculation of stresses on the boundary is not so straightforward. Symm (ref. 4), for example, developed an extrapolation scheme for predicting stresses on or close to the boundary based on the stresses within D (at some distance from L) known to be accurately calculated. A method of computation not requiring extrapolation is used in the present investigation, which leads to reasonably accurate boundary stresses.

A general representation of the second derivatives of $\chi(P)$ as $P \to p$ is not obtainable due to the strong singularity in the second derivatives of

$$\int_L \log|P - q| dq \ .$$

However, if only the total stress is considered

$$\theta = \sigma_x + \sigma_y = \nabla^2 \chi \ ,$$

then one can write

$$\theta(P) = \nabla^2[r^2(P) \cdot \sum_{i=1}^{m} \sigma_i \int_i \log|P - q|dq] = 4 \sum_{i=1}^{m} \sigma_i \int_i \log|P - q|dq$$

$$+ 2\nabla r^2(P) \cdot \sum_{i=1}^{m} \sigma_i \nabla \int_i \log|P - q|dq$$

as

$$\nabla^2 \int_i \log|P - q|dq = 0 , \qquad P \text{ in } D .$$

When $P \to p$ on L, $\theta(p)$ is well defined since the limiting values of all integrals can be obtained by using previously derived formulas.

Once θ is obtained on L, the stress components are determined from (3), by which one can show that

$$\tau_{xy} = - (\theta \frac{\partial x}{\partial n} \frac{\partial y}{\partial n} + F_x \frac{\partial y}{\partial n} + F_y \frac{\partial x}{\partial n}) . \tag{22}$$

If τ_{xy} is known, σ_x and σ_y can be calculated directly from (3).

NUMERICAL EXAMPLES

The examples presented are: 1) a circular disk subjected to diametrally opposite concentrated forces; and 2) an infinite media with an elliptic hole subjected to uniform internal pressure. Both examples have known analytic solutions, by which the accuracy of the numerical solutions may be conveniently assessed. Moreover, these examples illustrate significant characteristics of the numerical solutions. The first example shows the effect of extreme loading while the second illustrates that of boundary geometry.

An important simplification employed in both examples is the reduction of the number of unknowns through considerations of symmetry. The coordinate axes are assigned in such a way that the geometry and loading are symmetrical about both the x and y axes. By subdividing the boundary symmetrically, a similar symmetry in σ_i and μ_i can be obtained. Hence, if the total number of subdivisions around L is $2m$, then the number of equations and unknown source densities is reduced to m for interior problems and $m + 1$ for exterior problems.

Example 1. Circular Disk under Concentrated Loads

The analytic solution of this problem (ref. 5) is cited here for future reference (for notation, see figure 4):

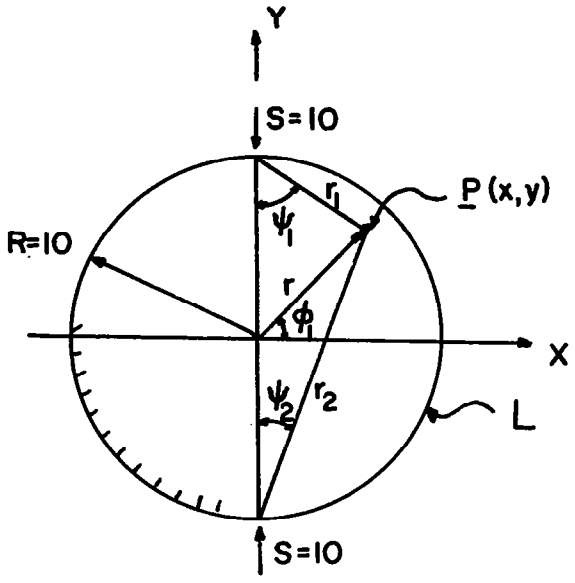

Figure 4.- Example 1, point loads on a circular disk.

$$\sigma_x + \sigma_y = \theta = \frac{-2S}{\pi}\left[\frac{\cos\psi_1}{r_1} + \frac{\cos\psi_2}{r_2} - \frac{1}{R}\right],$$

$$\sigma_y = \frac{-2S}{\pi}\left\{\frac{\cos^3\psi_1}{r_1} + \frac{\cos^3\psi_2}{r_2} - \frac{1}{2R}\right\},$$

$$\tau_{xy} = \frac{2S}{\pi}\left\{\frac{\sin\psi_1\cos^2\psi_1}{r_1} - \frac{\sin\psi_2\cos^2\psi_2}{r_2}\right\}.$$

For the numerical analysis, the boundary was subdivided into intervals of equal length h and the x and y axes intersected L at interval end points. Hence the geometry, loading, and subdivision of L is symmetric with respect to both axes, and the number of subdivisions per quadrant is denoted by k.

Equations (8) and (9) may be used to compute $\chi(p)$ and $\chi'(p)$ on the boundary. Choosing $s = s_0$ at $\phi_1 = \frac{\pi}{2}$, one obtains symmetrical boundary conditions;

$$\chi(p) = \begin{cases} -\frac{SR}{2}\cos\phi_1, & 0 < \phi_1 < \frac{\pi}{2} \\ \frac{SR}{2}\cos\phi_1, & \frac{\pi}{2} < \phi_1 < \frac{3\pi}{2} \\ -\frac{SR}{2}\cos\phi_1, & \frac{3\pi}{2} < \phi_1 < 2\pi \end{cases} \tag{23a}$$

$$\frac{\partial\chi(p)}{\partial n} = \begin{cases} \frac{S}{2}\cos\phi_1, & 0 < \phi_1 < \frac{\pi}{2} \\ -\frac{S}{2}\cos\phi_1, & \frac{\pi}{2} < \phi_1 < \frac{3\pi}{2} \\ \frac{S}{2}\cos\phi_1, & \frac{3\pi}{2} < \phi_1 < 2\pi \end{cases} \tag{23b}$$

Finally, the quantities $\frac{\partial x(p)}{\partial n}$ and $\frac{\partial y(p)}{\partial n}$ may be calculated from the following formulas

$$\left.\begin{aligned} \frac{\partial x(p)}{\partial n} &= -R\cos\phi_1 \\ \frac{\partial y(p)}{\partial n} &= -R\sin\phi_1 \end{aligned}\right\} \quad p \text{ on } L. \tag{24}$$

The source densities σ_i and μ_i $(i = 1, 2, \ldots k)$ are determined from equations (11) and (12) by using equations (23) and (24), subdivision length h and the coordinates of the interval center and end points. Stress components are calculated at field points on several circular arcs. The boundary $R = 10$ is denoted by C_0 and the arcs with $r = 9.75$, 9.5, 9.0, 8.0 and 6.0 by C_1, C_2, C_3, C_4, and C_5 respectively. Solutions are obtained for 4, 8, 16, 32 and 64 subdivisions per quadrant. The results are presented in tables 2 through 6 of Appendix B, in which both the exact and the numerical values of θ and σ_y are given. Presentation of the numerical results for each contour as a function of k is stopped once their convergence to within 1% has been obtained and an entry C is made in the tables.

The total stress is calculated directly from

$$\theta(P) = \nabla^2\chi(P)$$

$$= \nabla^2\left[r^2(P)\sum_{i=1}^{m}\sigma_i\int_i \log|P - q|dq\right]$$

so that μ_i does not enter into the calculation. Values of the total stress are shown, because the method of calculating the stresses at the boundary through equations (22) and (3) is dependent on the accuracy of θ. It may be noted that close to the boundary the accuracy of the computed values of θ are somewhat better than those of σ_y.

Tables 2 through 6 illustrate a number of special characteristics of the numerical solution. First of all, the convergence of the solution is slower in the region close to the boundary than in the region removed from the boundary, and in the region close to the point load than in the region away from it. Neither phenomena is unexpected. Both are related to the fact that the source densities are assumed to be piecewise constant. At a point close to the boundary, the stress is greatly affected by the boundary source densities in the immediate proximity and the local behavior of the source densities becomes critical. However, it becomes very difficult to represent this local behavior accurately by piecewise constant source densities. Likewise, in the region close to the point load ($x = 0$ and on the boundary), the piecewise constant source densities are not capable of accurately representing the actual situation.

In the major portion of the region convergence is obtained; that is, at those points in the region the computed values do not change as the number of subdivisions increases and the numerical solutions are in excellent agreement with known results. Note that one does not have to extend his computing facilities to the limit on every occasion. If convergence is obtained with a small number of subdivisions at all points of interest, calculations may be stopped with assurance that the results are accurate. If the arc lengths of the boundary intervals are compared with the distances of the various contours from the boundary, it is observed that the numerical solutions with tolerable accuracy are obtained at points which are at a distance greater than an interval length from the boundary.

Finally, the values of total stress calculated on the boundary, using $k = 64$, are an order of magnitude less than those values calculated on the contour C_1, except near $x = 0$. Therefore, the numerical results reflect quite well the physical condition that all stress components vanish on the boundary, except at $x = 0$ and $y = \pm 10$. The computation of boundary stresses will be considered in more detail in the next example.

Example 2. Infinite Plate with an Elliptic Hole

The problem of an infinite elastic media with an elliptic hole was considered by Symm (ref. 4) who applied a similar integral equation method. The same problem is also considered here to study the effect of boundary geometry on the accuracy of the numerical solution by varying the semi-axis ratio a/b. The geometry and notations relevant to this example are shown in figure 5.

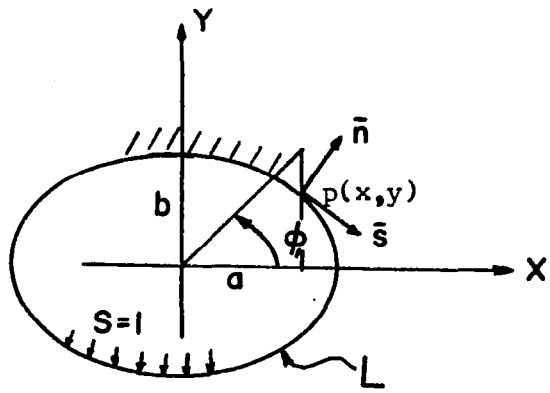

Figure 5.- Example 2, unit pressure on an elliptic hole.

The quantities calculated to illustrate the numerical results are the maximum shear stress τ and the normal stress σ_t tangent to the boundary. The analytical expressions for these quantities are given by (ref. 6):

$$\tau(P) = \left\{\left(\frac{\sigma_x - \sigma_y}{2}\right)^2 + \tau_{xy}^2\right\}^{\frac{1}{2}} = S\left[\frac{b^4x^2 + a^2y^2}{\left\{\left(x^2 + y^2 - c^2\right)^2 + 4c^2y^2\right\}^{\frac{3}{2}}}\right]^{\frac{1}{2}},$$

$$\sigma_t(p) = S\left(\frac{2\eta \cos \phi_1 - 3\eta^2 + 1}{\eta^2 - 2\eta \cos 2\phi_1 + 1}\right),$$

where

$$c^2 = a^2 - b^2, \qquad \eta = (a - b)/(a + b).$$

The coordinates of a point p on the boundary L are given by

$$x(p) = a \cos \phi_1, \qquad y(p) = b \sin \phi_1.$$

To preserve symmetry, the boundary is subdivided into equal intervals and the axes are drawn through the interval end points. One can then determine the stress function $\chi(P)$ represented in (14) by solving the $2k + 1$ equations generated from equations (15) through (17). The symmetrical canonical boundary conditions applicable to the problem are, from (8) and (9),

$$\chi(p) = -\frac{S}{2}(x^2 + y^2)$$

$$\frac{\partial \chi(p)}{\partial n} = -S\left(x\frac{\partial x}{\partial n} + y\frac{\partial y}{\partial n}\right).$$

The terms $\frac{\partial x}{\partial n}$ and $\frac{\partial y}{\partial n}$ are given by

$$\frac{\partial x}{\partial n} = x\left\{x^2 + \left(\frac{a}{b}\right)^4 y^2\right\}^{-\frac{1}{2}},$$

$$\frac{\partial y}{\partial n} = y\left\{\left(\frac{b}{a}\right)^4 x^2 + y^2\right\}^{-\frac{1}{2}}.$$

In order to illustrate the special characteristics of the numerical solution, the results are presented for $a/b = 1.5$, 2 and 5. Figure 11 of Appendix B presents the tangential stress σ_t calculated at the interval center points of the boundary of an ellipse with $a/b = 1.5$ and $a = 1.5$. Results are shown for $k = 8$ and 32, k being the number of subdivisions per quadrant. Note the improvement in accuracy as k increases. Slight fluctuations of the results with $k = 32$ are due to the assumption that the source densities are piecewise constant and to the ill-conditioning in the simultaneous equations used to determine σ_i and μ_i $(i = 1, 2, \ldots k)$. Both of these factors will be discussed later in some detail.

In figures 12 and 13 of Appendix B are presented the numerical values of σ_t for $k = 32$ for $a/b = 2$ and 5 respectively. A comparison of the calculated values of stress concentration at $x = a$ with the known analytical values reveals that the accuracy of the numerical solution decreases as a/b increases. These figures also illustrate the difference between the stress values calculated at interval center points and those at interval end points. Again the effect of the basic assumption that the source densities are piecewise constant is revealed. At an interval center point, the effect of this assumption, though significant, is generally tolerable. However, at interval end points, the approximate source density $\sigma(q)$ is discontinuous and, as such, creates an artificial situation at these points on the boundary. If one were to calculate σ_t at all points on the boundary, in general the numerical solution would be in greatest error at the interval end points.

In figure 14 are plotted the values of $10\sigma_i h$ for $k = 32$ and for $a/b = 2$ and 5. The data points are plotted at each interval center point and a smooth curve is drawn through them. The quantity $\sigma_i h$ is chosen as it is independent of the circumference of an ellipse for a given a/b ratio. This parameter as plotted in figure 14 may be interpreted as a comparison of the source densities for two ellipses with the same circumferential length but with different a/b ratios. Note that, if the circumferences are equal, then the total load applied to the internal boundary is the same in both cases. Hence any difference in the stress distributions in the two media are entirely due to the difference in the boundary geometry.

Figure 14 illustrates quite clearly why better accuracy may be expected in the case of $a/b = 2$ than in the case of $a/b = 5$. The rate of change of the source density σ for $a/b = 2$ is much less than that for $a/b = 5$ for virtually all values of x. Hence, the assumption that $\sigma(q)$ is piecewise constant is more justifiable in the former case than in the latter. Similarly, if σ were plotted for $a/b = 1.5$, one would find still less variation than when $a/b = 2.0$. The numerical results (figure 11) reflect this circumstance.

Figures 12, 13 and 14 illustrate that the accuracy of the computed stresses at both the interval end and center points is in most instances directly related to the rate of change of σ with respect to x. It is also noted that the numerical results at interval end points are much more sensitive to the rate of change of σ than those at interval center points. This phenomenon indicates that the basic assumption of piecewise constant source densities is a limiting factor in the application of this numerical method.

It appears that the presence of a stress concentration (at $x = a$) does not, in itself, lead to the inaccurate results at that point. The relatively large error at $x = 0$ should be considered in terms of the variation in σ in the neighborhood of $x = 0$. At those points where the rate of change of σ is large, a relatively large error in stresses is observed even though the rate of change in stresses at such points is much less than that at $x = a$.

Some additional results for the exterior problem of an ellipse with $a/b = 5$ are presented in tables 7, 8 and 9, for $k = 4$, 8, 16 and 32. Numerical results are presented at points on contours described by

$$\frac{x^2}{(a + \delta)^2} + \frac{y^2}{(b + \delta)^2} = 1 ,$$

contours C_1, C_2 and C_3 corresponding to the cases of $\delta/a = 0.1$, 0.06 and 0.04 respectively. Each of these contours has the property that they are everywhere approximately a distance δ away from the boundary. Hence, the tables show the convergence characteristics of the numerical solution as the field points uniformly approach the boundary. As in the case of the interior problem, excellent results are obtained in the region where δ/a is greater than h/a.

So far little has been said about the magnitude of the computational work involved. It has been learned that the numerical technique presented in this report is quite economical with respect to computer time. For example, the total time required on an IBM 7044 system to solve the exterior problem of ellipse with $a/b = 5$ for $k = 4$, 8, 16 and 32 was about eight minutes. This included the calculation of both the boundary and the field stresses.

However, setting-up of a reliable computational program was not always so straightforward. For example, one of the exterior problems with $k = 32$ was reduced to that of solving a set of sixty-five simultaneous equations, and it became a problem of tackling an ill-conditioned matrix. The effect of matrix ill-conditioning is evidenced by the random fluctuations of the solution for the exterior problem with $a/b = 1.5$ and $k = 32$; see figure 11. In the case of $a/b = 2$ and 5, the problem of ill-conditioning was somewhat alleviated by using some scaling in the coefficient matrix and trying various subroutines. Nevertheless, ill-conditioning was still a problem in those computations and it was not possible to extend the number of boundary subdivisions from 32 to 48 in any of the exterior problems. It is a conclusion of this investigation as well as of others (refs. 1, 2, 3 and 4) that the present formulation of the numerical scheme will inherently lead to the circumstance that the simultaneous equations governing the σ_i and μ_i become ill-conditioned as the number of boundary subdivisions increases. Therefore, if one were to increase the number of boundary subdivisions, he would have to make a substantial increase in the computational precision.

CONCLUDING REMARKS AND RECOMMENDATIONS

An integral equation method for solving the first fundamental boundary-value problem of plane elastostatics is presented. As illustrated through numerical examples, the principal advantages of this method are its simplicity and generality. This powerful method is likely to provide a new avenue of solution for some of the complicated biharmonic boundary-value problems, which are not amenable to any other treatment.

In order to study the practical applicability of this method, two typical example problems -- one with an extreme loading condition and the other with variable geometry -- are investigated. In both cases, excellent results are obtained everywhere in the region, except in the close neighborhood of the boundary (at a distance less than an interval length from the boundary). The following conclusions are drawn from this investigation:

1). Once the convergence of a numerical solution has been established at a point, the error in the numerical results may be expected to be less than one percent.

2). In general, the convergence of a numerical solution is obtained less rapidly in regions near the boundary than in areas removed from it.

3). The accuracy and convergence of the stresses computed at the boundary are directly related to the rate of change of the source density at

the boundary.

4). Matrix ill-conditioning may occur before the convergence of the stresses at or near the boundary can be established.

5). The main cause of matrix ill-conditioning, which occurs as the number of boundary subdivisions is increased, seems to lie in the basic assumption that the source density functions are piecewise constant on the boundary.

Based on these conclusions, two recommendations are in order. The first one is to introduce a more general assumption on the source density functions; i.e., they will be assumed to be piecewise linear within each boundary subdivision instead of piecewise constant. The second is to make a further refinement in the computational scheme for the purpose of alleviating the problem of matrix ill-conditioning. The results of the further investigation will be reported in a sequel to this report.

APPENDIX A. ACCURACY OF NUMERICAL INTEGRATIONS

The accuracy of the approximate integration formulas is illustrated by comparing approximate and exact results calculated from the model shown in figure 6. The model consists of a line segment of length h inclined at an angle α to the x-axis. The field point P(x,y) is a distance ε away from the segment.

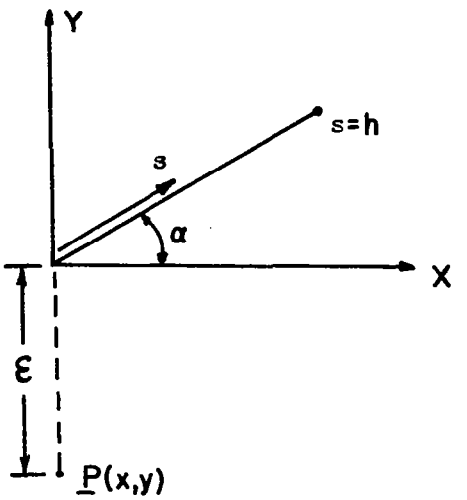

Figure 6.- Analytical model.

If the line segment represents a boundary subdivision, then the integral

$$I = \int_i \log |P - q| \, dq$$

and its derivatives may be written as

$$I = \frac{1}{2} \int_0^h \log (s^2 + \varepsilon^2 + 2s \, \varepsilon \sin \alpha) \, ds$$

$$I_x = \int_0^h \frac{-s \cos \alpha \, ds}{s^2 + \varepsilon^2 + 2s \, \varepsilon \sin \alpha}$$

$$I_y = \int_0^h \frac{-(\varepsilon + s \sin\alpha)\, ds}{s^2 + \varepsilon^2 + 2s\,\varepsilon \sin\alpha}$$

and $$I_{xx} = -I_{yy} = \int_0^h \frac{[(\varepsilon + s \sin\alpha)^2 - s^2 \cos^2\alpha]\, ds}{(s^2 + \varepsilon^2 + 2\varepsilon\, s \sin\alpha)^2}$$

where the coordinate s is defined in figure 6 and subscripts on I denote differentiation with respect to the subscripted variable.

Performing the indicated integrations, one obtains

$$I = \frac{1}{2}(h + \varepsilon \sin\alpha) \log (h^2 + \varepsilon^2 + 2h\,\varepsilon \sin\alpha) - \varepsilon \sin\alpha \log \varepsilon - h$$

$$- \varepsilon \cos\alpha \cdot \tan^{-1}\left(\frac{\varepsilon \cos\alpha}{h + \varepsilon \sin\alpha}\right)$$

$$I_x = -\cos\alpha \left[\frac{1}{2} \log (h^2 + \varepsilon^2 + 2h\varepsilon \sin\alpha) - \frac{1}{2} \log \varepsilon^2\right] + \sin\alpha \tan^{-1}\left(\frac{h + \varepsilon \sin\alpha}{\varepsilon \cos\alpha}\right)$$

$$- \alpha \sin\alpha$$

$$I_y = -\sin\alpha \left[\frac{1}{2} \log (h^2 + \varepsilon^2 + 2h\varepsilon \sin\alpha) - \frac{1}{2} \log \varepsilon^2\right]$$

$$- \cos\alpha \left[\tan^{-1}\left(\frac{h + \varepsilon \sin\alpha}{\varepsilon \cos\alpha}\right) - \alpha\right]$$

$$I_{yy} = -I_{xx} = \frac{\varepsilon \sin\alpha + h(\sin^2\alpha - \cos^2\alpha)}{h^2 + \varepsilon^2 + 2\varepsilon h \sin\alpha} - \frac{\sin\alpha}{\varepsilon}$$

In all cases, Simpson's rule was used to determine approximate integration formulas. The formulas so derived are implicitly defined in the following manner. If

$$H = \int_i f(P,q)\, dq\ ,$$

then by Simpson's rule one has

$$H \approx \frac{h}{6}\left[f(P,q_{i-1/2}) + 4f(P,q_i) + f(P,q_{i+1/2})\right] .$$

Specific formulas are developed by substituting the appropriate values of the integrands into the preceding equation.

In the following figures, exact and approximate variables are superscripted with E and A respectively. The accuracy of the approximate formulas is illustrated by means of tables and curves showing

$$T = I^A/I^E - 1 , \qquad T_x = I_x^A/I_x^E - 1 , \qquad T_y = I_y^A/I_y^E - 1 ,$$

and $T_{yy} = I_{xx}^A/I_{xx}^E - 1$. Note that $T_{yy} = T_{xx}$.

Table 1.- Accuracy of I^A for $\alpha = 0.0$

H = 4

ε/h	T
2.5	-.00001
1.25	-.00004
.75	.001
.5	.007
.25	.03
.125	-.2

H = 1

ε/h	T
2	-.00009
1	.001
.5	-.02
.25	-.04

H = .5

ε/h	T
4	-.00001
2	-.002
1	-.0003
.5	-.007
.25	-.02

H = .25

ε/h	T
2	.0001
1	-.0002
.5	-.004
.2	.015

H = .1

ε/h	T
2.5	.00002
1.25	.00004
0.5	-.003
.25	-.009

H = .05

ε/h	T
2.5	.00002
1.0	-.00006
.5	-.002

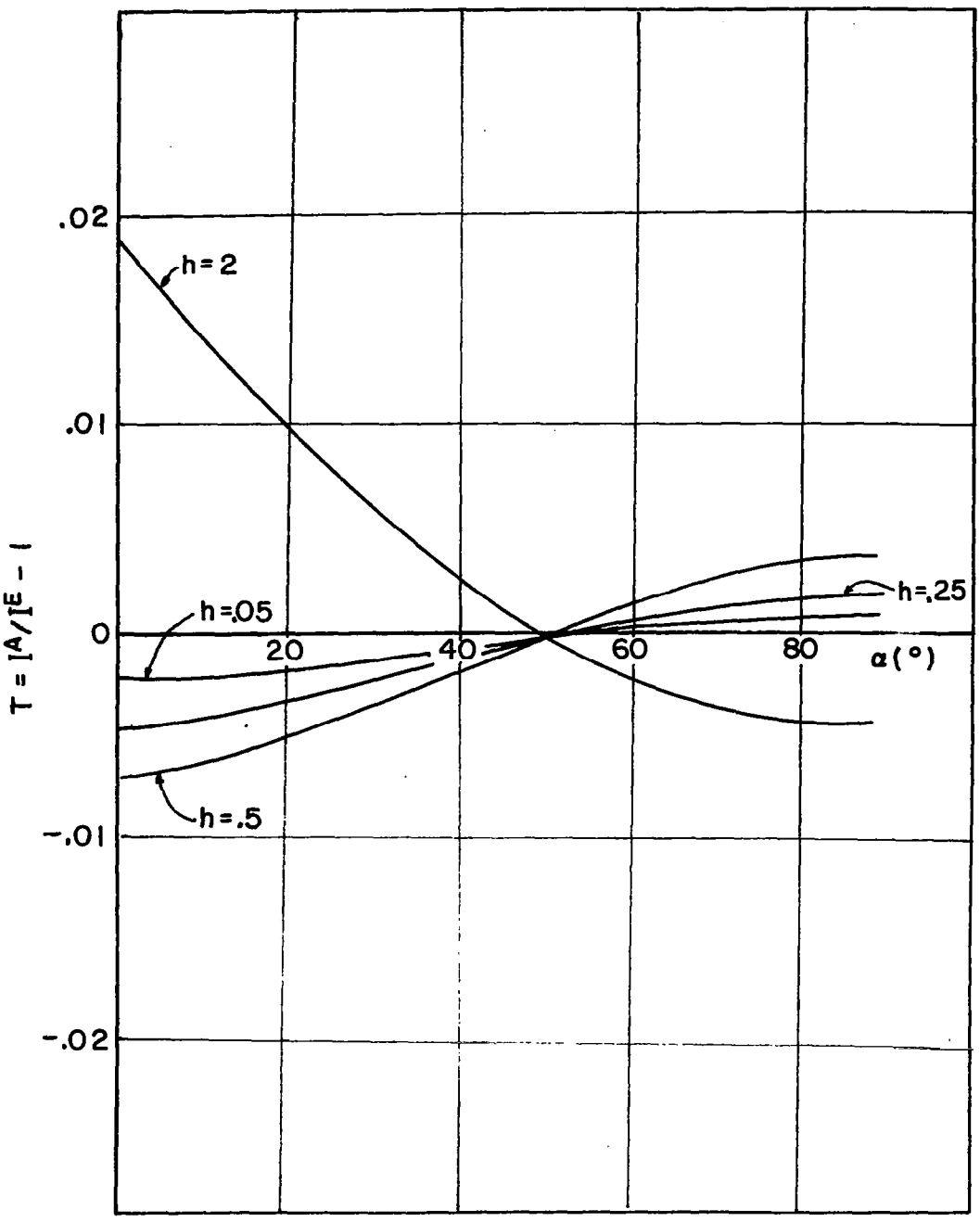

Figure 7.- Accuracy of I^A for $\varepsilon/h = 0.5$.

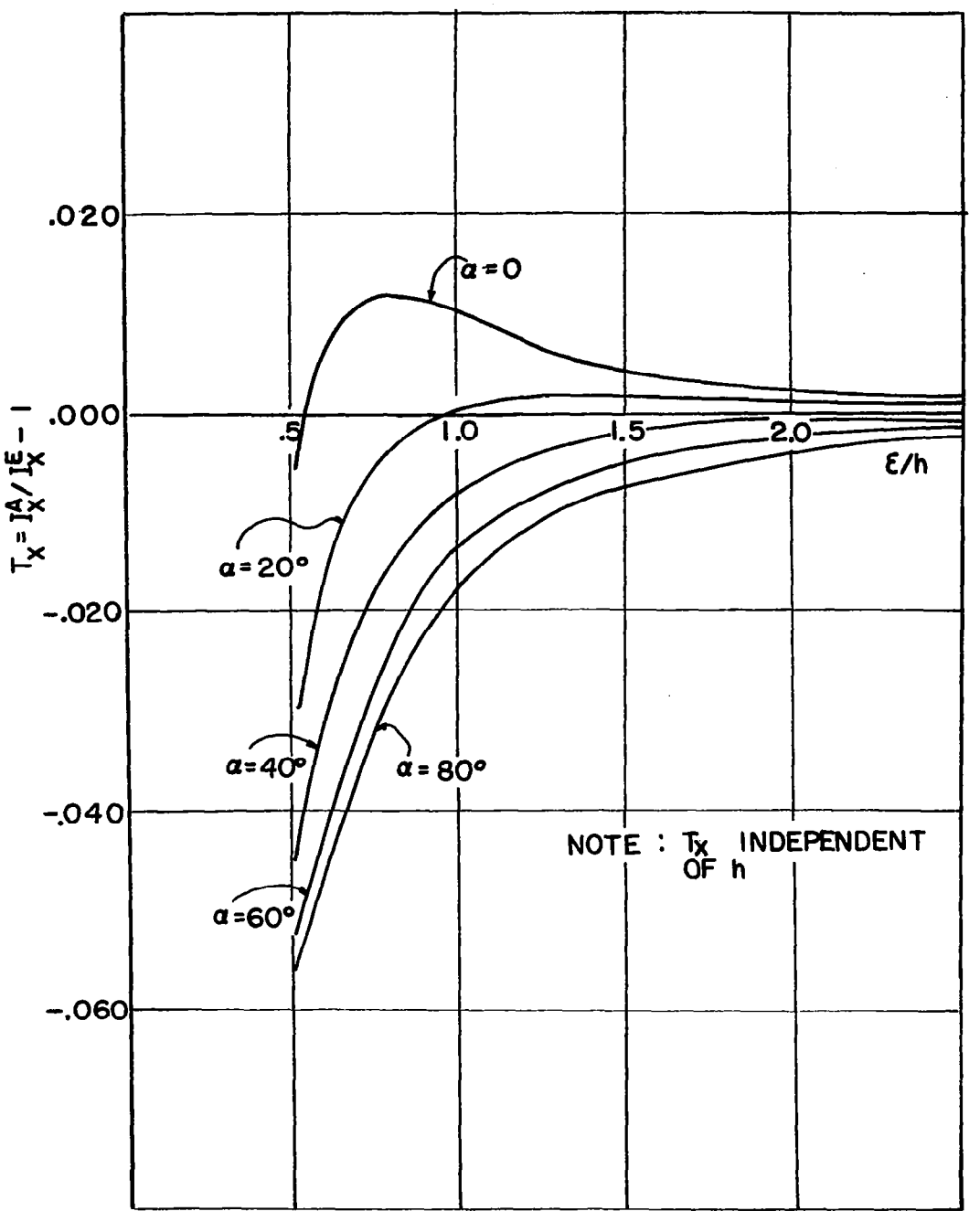

Figure 8.- Accuracy of I_x^A.

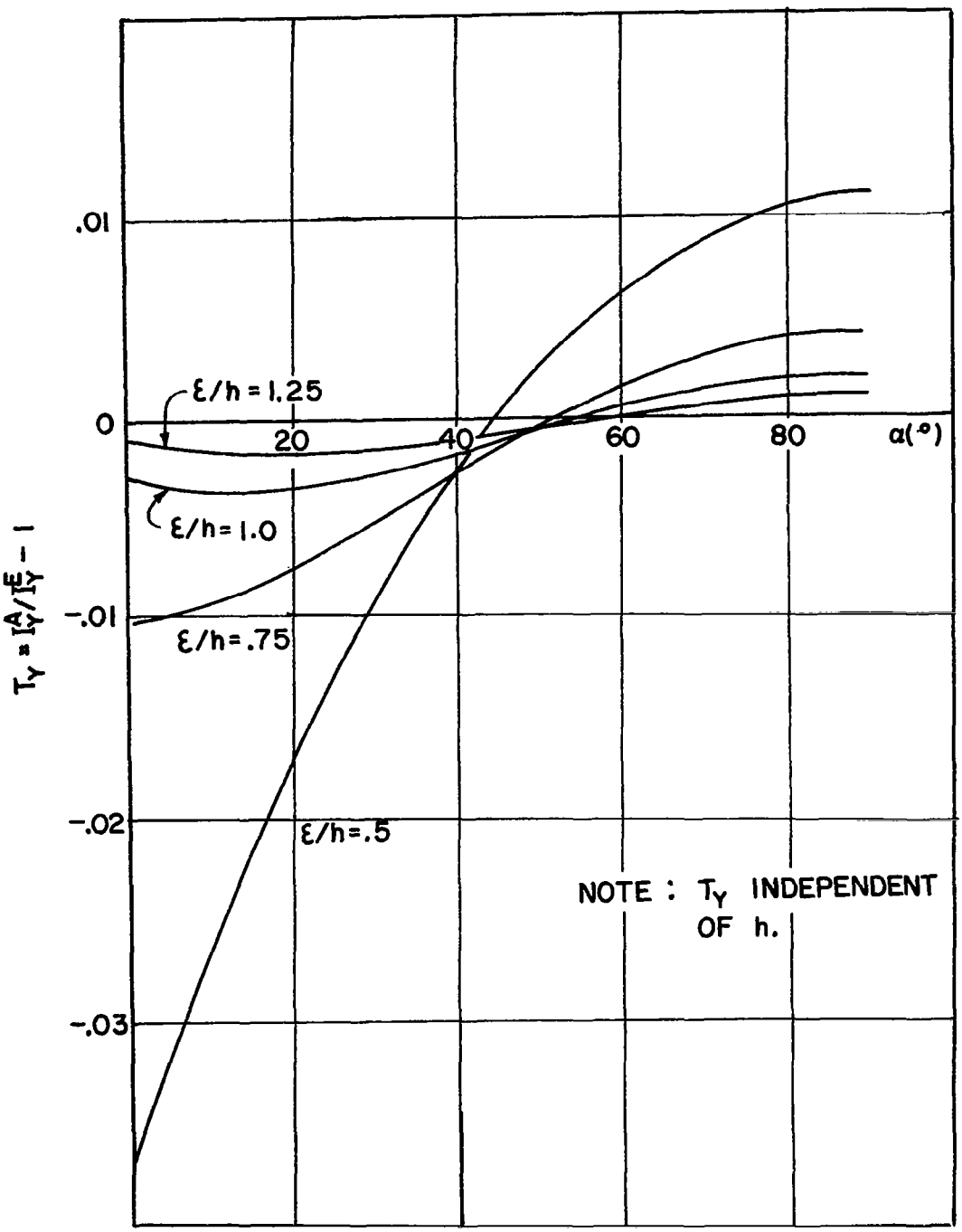

Figure 9.- Accuracy of I_y^A.

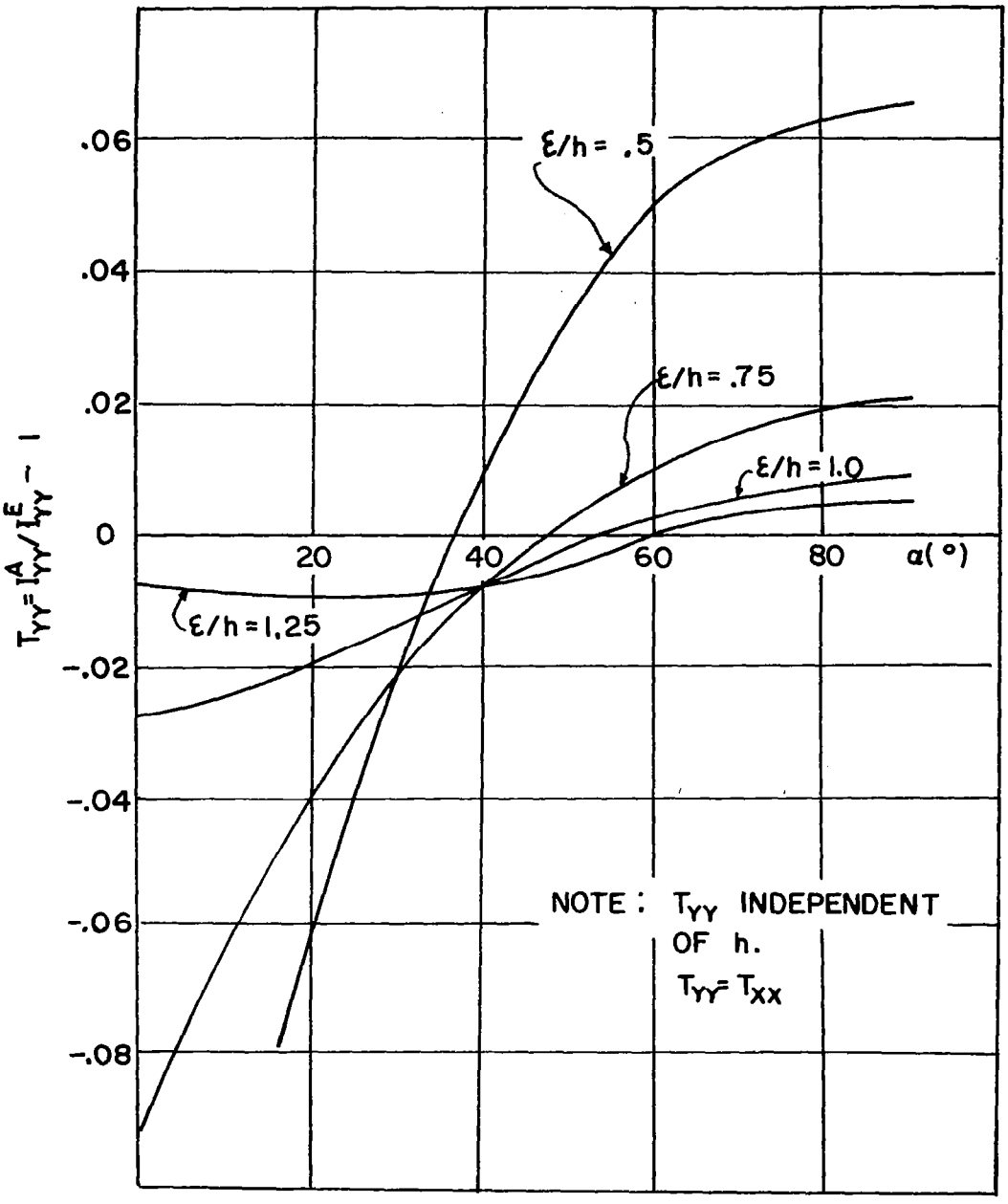

Figure 10.- Accuracy of I^{A}_{yy}.

APPENDIX B. COMPARISON OF ANALYTICAL AND NUMERICAL STRESS VALUES

Numerical results of the two example problems are presented in this Appendix. Numerical values of the stresses for the first example, namely the problem of a circular disk subjected to a pair of diametrally opposite concentrated loads, are given in tables 2 through 6. The exact analytical solutions are also listed for comparison. Numerical results of the second example, namely an infinite plate with an elliptic hole subjected to a constant internal pressure, are presented in figures 11 through 14 and tables 7 through 9. For the purpose of comparison, the existing analytic solutions are also made available in the figures and the tables.

Table 2.- Stresses at contour C_5: $(x^2 + y^2)^{\frac{1}{2}} = 6.0$; circular disk.

x	$-\theta$				$-\sigma_y$				
	EXACT	NUMERICAL			EXACT	NUMERICAL			
		K = 4	8	16			8	16	32
6.00	.2996	.2956	.2988	C	.3701	.3646	.3694	C	C
5.54	.3382	.3349	.3377	C	.3981	.3945	.3978	C	C
4.24	.4905	.4974	.4915	C	.5232	.5542	.5251	C	C
2.30	.8930	.9468	.9007	C	.9660	1.062	.9818	C	C
1.17	1.193	1.182	1.196	C	1.402	1.282	1.393	C	C
0.0	1.353	1.273	1.343	C	1.671	1.331	1.607	1.661	C

Table 3.- Stresses at contour C_4: $(x^2 + y^2)^{\frac{1}{2}} = 8.0$; circular disk.

x	$-\theta$					$-\sigma_y$				
	EXACT	NUMERICAL				EXACT	NUMERICAL			
		K = 4	8	16	32		K = 4	8	16	32
8.00	.1397	.1395	.1382	.1395	C	.1551	.0426	.1462	.1549	C
7.39	.1624	.1661	.1610	.1622	C	.1627	.1049	.1580	.1626	C
5.66	.2666	.2217	.2651	.2665	C	.2014	.1787	.2031	.2017	C
3.06	.7451	1.121	.7503	.7464	.7455	.4580	.9817	.4621	.4611	.4591
1.56	1.656	1.851	1.805	1.673	1.657	1.304	1.814	1.627	1.345	1.309
0.0	2.900	1.991	2.611	2.852	2.894	3.218	1.161	2.423	3.054	3.193

Table 4.- Stresses at contour C_3: $(x^2 + y^2)^{\frac{1}{2}} = 9.0$; circular disk.

x	$-\theta$					$-\sigma_y$				
	EXACT	NUMERICAL				EXACT	NUMERICAL			
		K = 8	16	32	64		K = 8	16	32	64
9.00	.0668	.0752	.0669	.0669	C	.0703	-.1144	.0537	.0703	C
8.31	.0782	.0870	.0783	.0783	C	.0722	-.0247	.0636	.0722	C
6.36	.1322	.1410	.1323	.1323	C	.0813	.1104	.0844	.0814	C
3.44	.4290	.3331	.4277	.4291	C	.1470	-.0366	.1443	.1480	.1474
1.76	1.377	2.148	1.377	1.379	C	.5355	1.269	.4737	.5402	.5376
0.0	6.064	3.928	5.349	5.936	6.046	6.383	2.048	4.664	6.013	6.325

Table 5.- Stresses at contour C_2: $(x^2 + y^2)^{\frac{1}{2}} = 9.5$; circular disk.

x	$-\theta$				$-\sigma_y$			
	EXACT	NUMERICAL			EXACT	NUMERICAL		
		K = 16	32	64		K = 16	32	64
9.50	.0326	.044	.0331	.0327	.0335	- .3	-.0004	.0334
8.78	.0383	.049	.0388	.0383	.0339	- .15	.016	.0339
6.71	.0651	.078	.0657	.0651	.0360	.066	.0394	.0361
3.63	.2197	.233	.2204	.220	.0506	- .11	.0365	.0509
1.85	.8038	.597	.8014	.8041	.1383	- .622	.0912	.1398
0.0	12.42	7.831	10.85	12.13	12.74	3.694	9.16	11.96

Table 6.- Stresses at contour C_1: $(x^2 + y^2)^{\frac{1}{2}} = 9.75$; circular disk.

x	$-\theta$			$-\sigma_y$		
	EXACT	NUMERICAL		EXACT	NUMERICAL	
		K = 32	64		K = 32	64
9.75	.0161	.0278	.0167	.0163	-.657	-.052
9.01	.0189	.0311	.0195	.0164	-.356	-.021
6.89	.0322	.0464	.0329	.0169	.046	.0203
3.73	.1099	.1290	.1110	.0203	-.351	-.0162
1.92	.4166	.4344	.4179	.0377	-1.04	-.0720
0.0	25.15	15.6	21.87	25.46	6.69	18.11

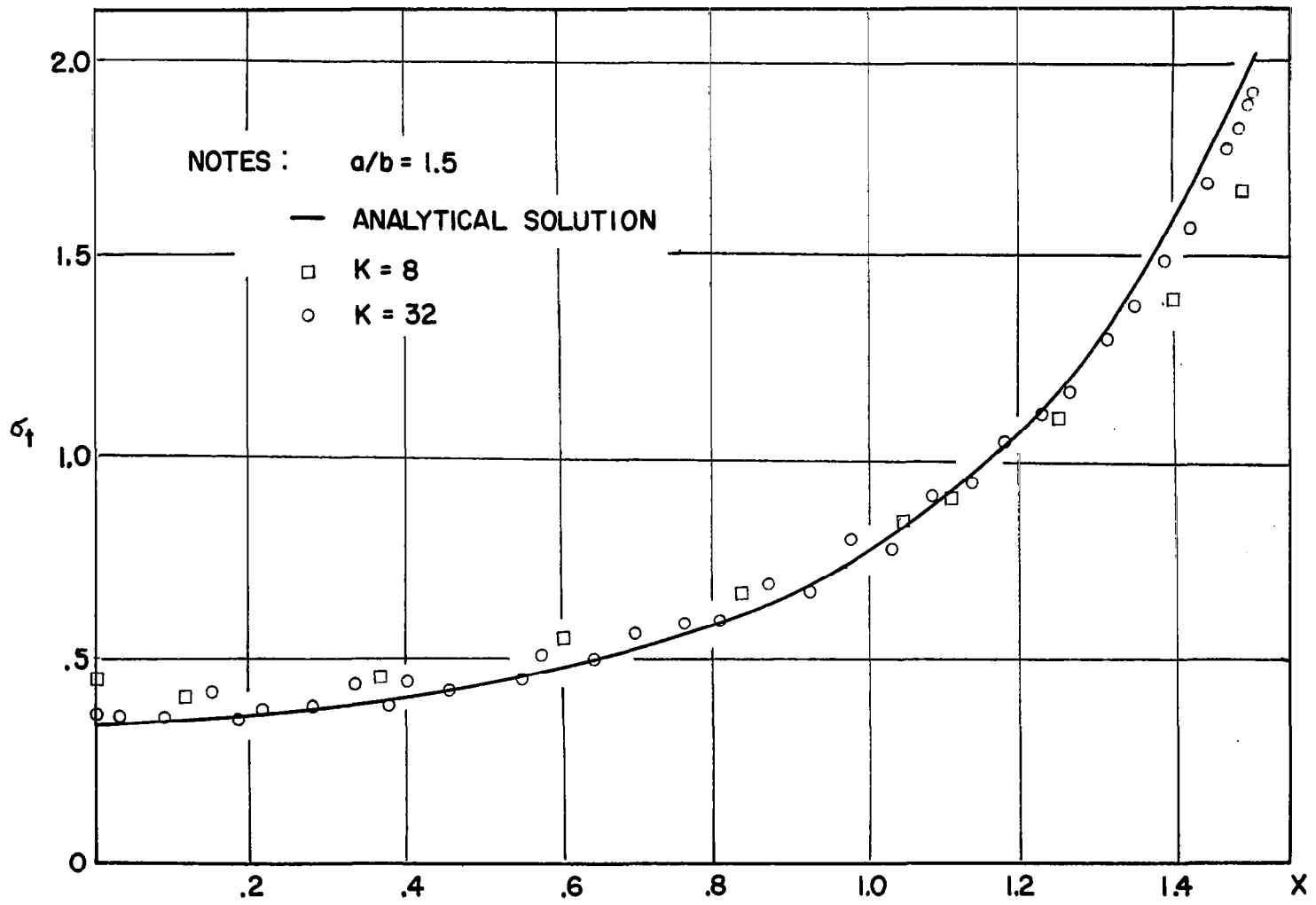

Figure 11.- Tangential stress at the elliptic boundary.

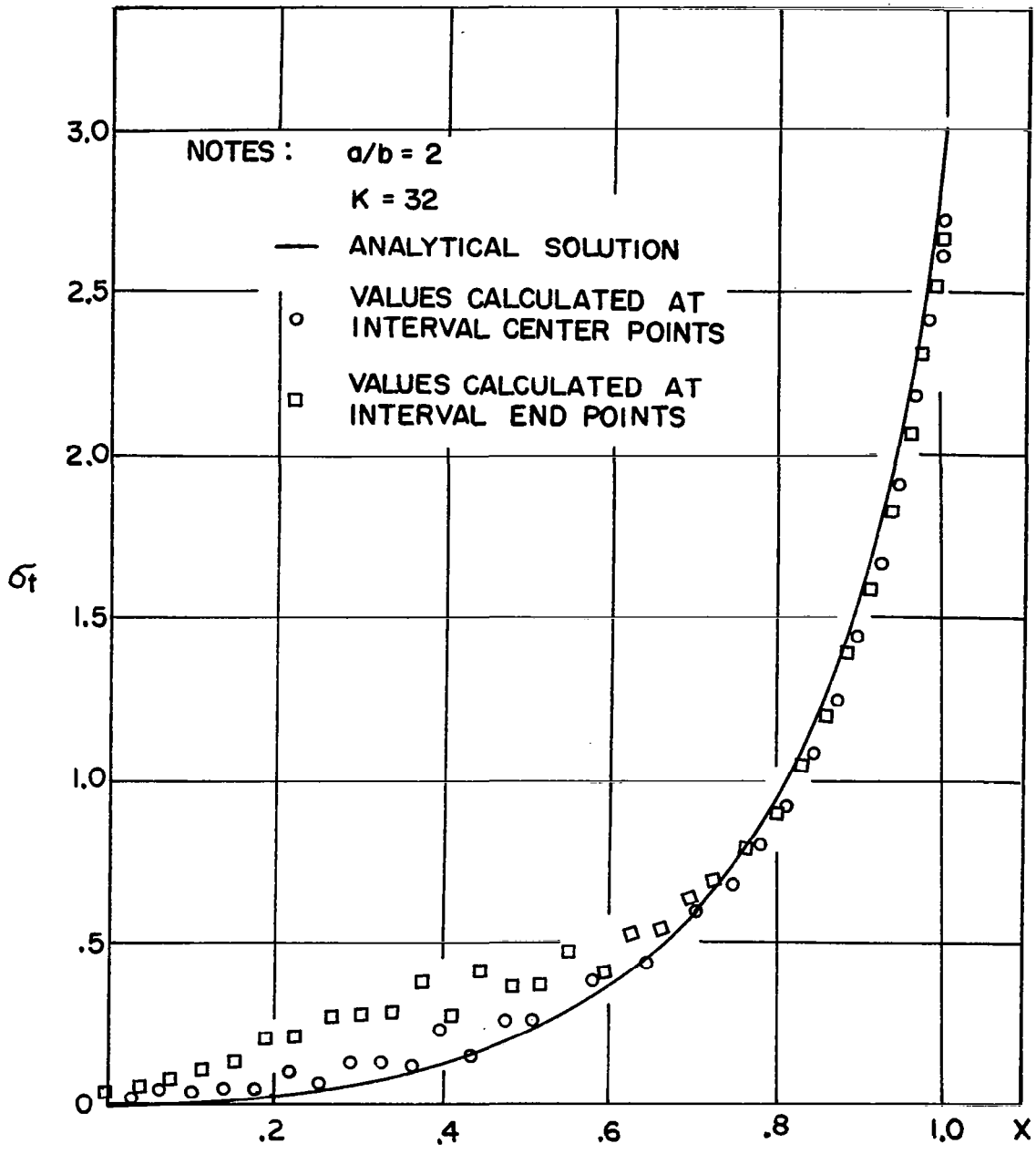

Figure 12.- Tangential stress at the elliptic boundary.

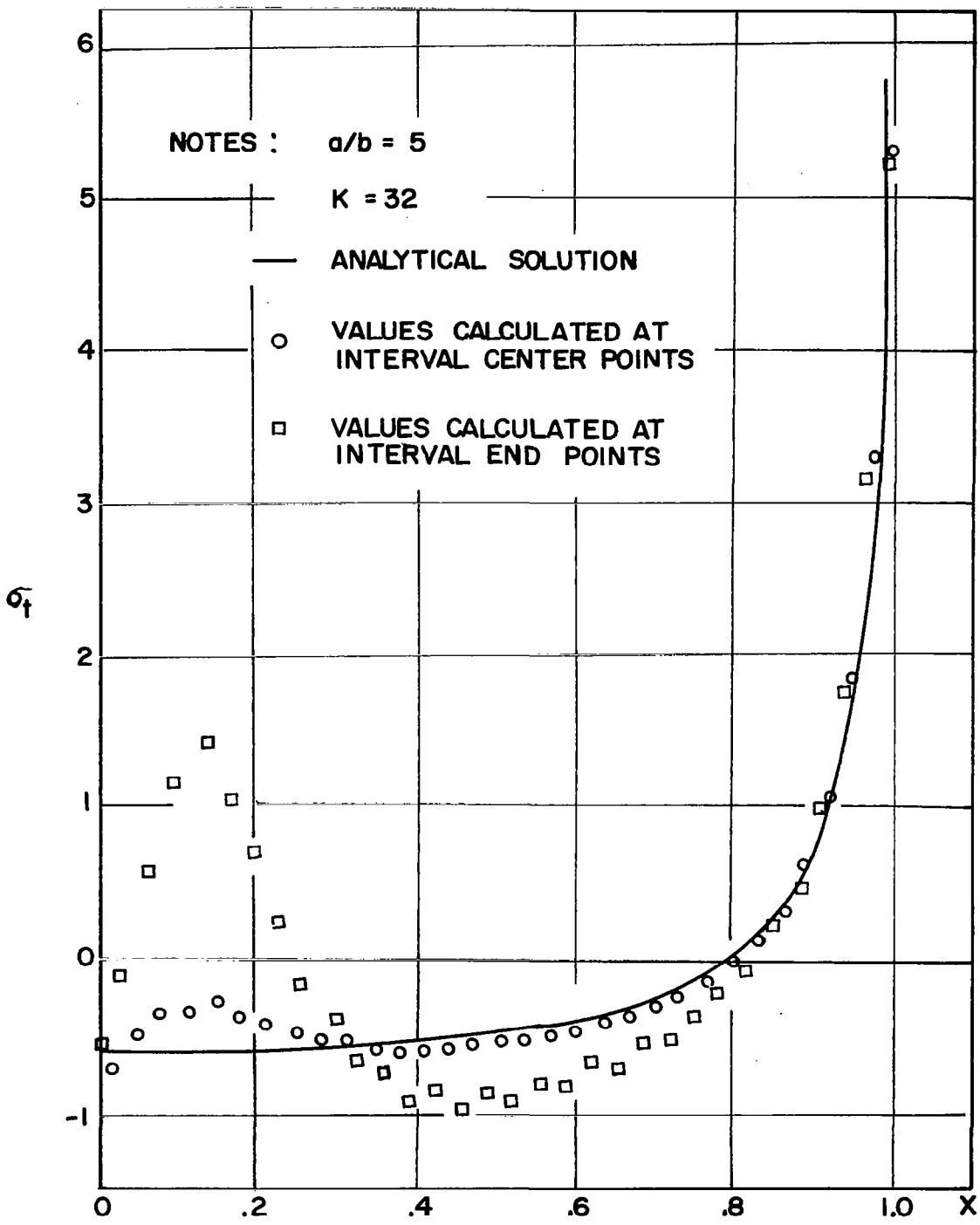

Figure 13.- Tangential stress at the elliptic boundary.

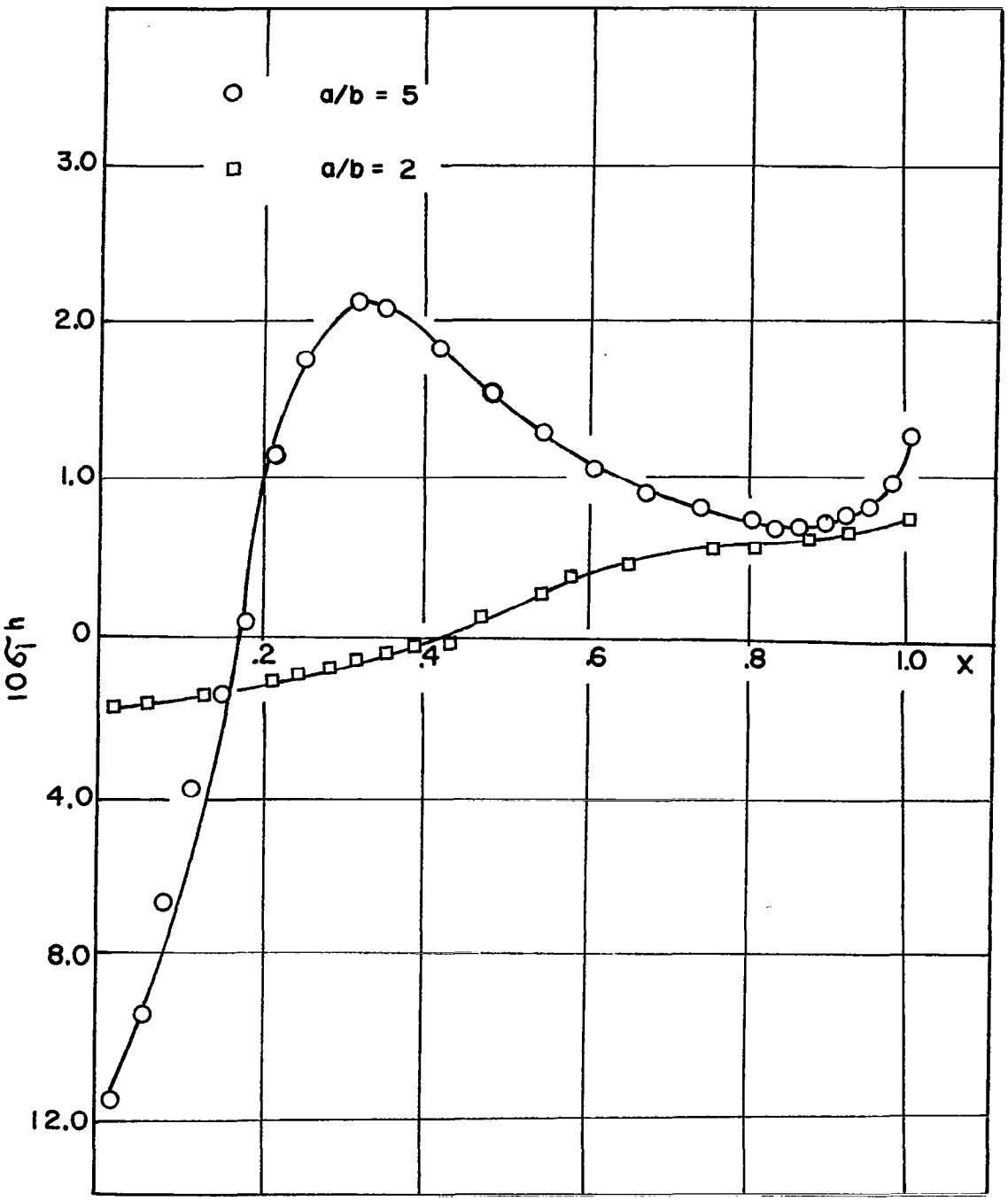

Figure 14.- Variation of source densities.

Table 7.- Numerical values of τ on the contour C_1: $\frac{\delta}{a} = 0.1$
(Elliptic hole with $\frac{a}{b} = 5$)

x/a	Maximum Shear Stress τ				
	EXACT	NUMERICAL			
		K = 4	8	16	32
1.100	.3520	.345	.3551	.3582	.3522
1.079	.6304	.888	.5702	.6114	.6287
1.016	1.030	1.05	1.082	1.034	1.030
.915	.8594	2.271	.8221	.8593	.8600
.778	.5742	1.408	.5276	.5718	.5742
.611	.4130	.7033	.3516	.4152	.4131
.421	.3303	1.347	.4095	.3340	.3313
.215	.2907	.937	.2907	.2928	.2911
.000	.2798	1.278	.3259	.2589	.2814

Table 8.- Numerical values of τ on the contour C_2: $\frac{\delta}{a} = 0.06$
(Elliptic hole with $\frac{a}{b} = 5$)

x/a	Maximum Shear Stress τ			
	$\tau_{anal.}$	$\tau_{numerical}$		
		K = 8	16	32
1.060	.6407	.461	.6478	.6413
1.040	1.040	.960	.9849	1.040
.979	1.240	1.721	1.197	1.240
.881	.7977	.475	.8464	.7966
.749	.5078	.232	.5388	.5064
.589	.3655	.482	.3730	.3646
.406	.2941	.473	.3316	.2949
.207	.2598	.512	.2411	.2636
.000	.2496	1.366	.2884	.2475

Table 9.- Numerical values of τ on the contour C_3: $\frac{\delta}{a} = .04$
(Elliptic hole with $\frac{a}{b} = 5$)

x/a	Maximum Shear Stress τ			
	$\tau_{anal.}$	$\tau_{numerical}$		
		K = 8	16	32
1.04	.981	.41	.957	.986
1.02	1.431	1.39	1.336	1.449
.961	1.280	2.11	1.044	1.302
.865	.741	.40	.920	.756
.735	.469	.86	.678	.474
.578	.339	1.40	.352	.323
.398	.274	.327	.414	.283
.203	.243	1.67	.064	.240
.000	.239	1.1	.973	.169

REFERENCES

1. Jaswon, M. A., "Integral Equation Methods in Potential Theory. I," Proc. Roy. Soc. Ser. A., Vol. 275, 1963, pp. 23-32.

2. Symm, G. T., "Integral Equation Methods in Potential Theory. II," Proc. Roy. Soc. Ser. A., Vol. 275, 1963, pp. 33-46.

3. Jaswon, M. A. and Ponter, A. R., "An Integral Equation Solution of the Torsion Problem," Proc. Roy. Soc. Ser. A., Vol. 273, 1963, pp. 237-246.

4. Symm, G. T., "Integral Equation Methods in Elasticity and Potential Theory," National Physical Laboratory, Mathematics Division, London, Dec. 1964.

5. Muskhelishvili, N. I., Some Basic Problems of the Mathematical Theory of Elasticity, N. V. P. Noordoff, Groningen, Holland, 1953.

6. Sokolnikoff, I. S., Mathematical Theory of Elasticity, McGraw-Hill Book Company, New York, 1956.

NASA-Langley, 1967 — 32 CR-779